*Journal of Nano- and Electronic Physics*
Vol. **12** No 6, 06009(5pp) (2020)

*Журнал нано- та електронної фізики*
Том **12** № 6, 06009(5cc) (2020)

# Influence of $Mn^{2+}$ Substitution on the Optical Properties of Novel $CaLi_2O_2$ Nanoparticles Synthesized by Sol-gel Method

A. Kadari[1,*], A. Azaiz[2], N. Mokhtari[1], D. Horri[1]

[1] *Engineering Physics Laboratory, University of Tiaret, Algeria*
[2] *Synthesis and Catalysis Laboratory, University of Tiaret, Algeria*

(Received 14 August 2020; revised manuscript received 15 December 2020; published online 25 December 2020)

A novel calcium lithium composite oxide $CaLi_2O_2$ nanoparticle has been successfully synthesized by using sol-gel method. The objective of the present work is to examine the change of optical properties with the change of $Mn^{2+}$ ion concentration in $CaLi_2O_2$ nanoparticles. The novelty of this study is the synthesis of Mn-doped $CaLi_2O_2$ nanoparticles. In order to investigate their physical properties the resulting samples in powder form were thermally treated at 300 °C and then characterized by powder X-ray diffraction (XRD), UV-Visible (UV-Vis) spectroscopy and Fourier Transform Infrared spectroscopy (FT-IR). The XRD patterns show that the crystalline structure has been changed with the change of $Mn^{2+}$ ion concentration in $CaLi_2O_2$ lattice. The incorporation of manganese atoms into $CaLi_2O_2$ has been confirmed by the FT-IR spectroscopy. This may be explained by the apparition of some absorption bands in the wavenumber range from 584 to 601 $cm^{-1}$. The particles size decreases from 463 Å to 117 Å. The band gap values were tuned from 3.769 eV to 3.794 eV and discussed based on the quantum confinement effect.

**Keywords:** Sol-gel, $CaLi_2O_2$, $Mn^{2+}$ doping, Band gap.

DOI: 10.21272/jnep.12(6).06009 PACS numbers: 81.20.Fw, 82.33.Ln

## 1. INTRODUCTION

The use of Li-CaO oxide in the transesterification reaction and in the catalytic activity was investigated by Watkins et al. [1]. The capture of carbon dioxide by transition metal aluminates, calcium aluminate, calcium zirconate, calcium silicate and lithium zirconate has been studied previously by several authors [2-4]. Biological, mechanical and physical properties of electrophoretically deposited lithium-doped calcium phosphates were investigated by Drdlid et al. [5]. The potential application of this work is to use the $Mn^{2+}$ doped $CaLi_2O_2$ nanoparticles in the field of thermoluminescence dosimetry. Several papers have been reported the influence of $Mn^{2+}$ ions on the physical properties of different materials such as ZnS [6], LiF-$Sb_2O_3$-ZnO-$B_2O_3$-$SiO_2$ glasses [7], $TiO_2$ [8], and $Cd_{0.9-x}Mn_xZn_{0.1}S$ [9].

The doping of manganese ions with different oxide nanoparticles provided better optical and photoluminescence properties and these were observed in many published papers. $Mn^{2+}$ doping gave the possibility to tune for a wide range of the band gap of the studied material.

Doping of various materials by manganese ions ($Mn^{2+}$) completely reduces the emission of surface states and improves their emission activity. It is well known that surface state plays an important role in the trapping of excited carriers in nanoparticles during the emission process, and then they transfer the energy from these last into the dopant centers [10, 11].

Recently, different physical and chemical preparation techniques, such as hydrothermal followed by calcination, the Pechini process, solid state routes, oxalate-precursor co-precipitation and spray pyrolysis method are employed to prepare materials in powder form composed of nanoparticles. Sol-gel process is one of the effective methods for the synthesis of metal oxide nanoparticles because it has many advantages over other methods [12, 13].

In the present investigation, $CaLi_2O_2$ nanoparticles were synthesized by sol-gel method. The effect of Mn dopant on the structural and optical properties has been studied and discussed in detail. The objective of the present work is to examine the change in the optical properties with the change of $Mn^{2+}$ ion concentration in $CaLi_2O_2$ nanoparticles.

## 2. MATERIALS AND METHODS

### 2.1 Materials

Calcium lithium composite oxide $CaLi_2O_2$ nanoparticles were synthesized using sol-gel method for the first time in this study. All reagents were of analytical grade and were used without further purification. For the synthesis of this oxide, the following precursors were used: calcium nitrate ($Ca(NO_3)_2$, 99 % Sigma-Aldrich) and lithium nitrate ($LiNO_3$, 99 % Sigma-Aldrich). For the doping step, manganese acetate ($Mn(CH_3CO_2)_2.2H_2O$, 99 % Sigma-Aldrich) has been used as a precursor. Distilled water was used as a solvent and urea ($CH_4N_2O$) was used as a catalyst.

### 2.2 Powder Preparation by Sol-gel Processing

In order to synthesize $CaLi_2O_2$ nanoparticles via sol-gel method the precursor reacts with the solvent (distilled water) to form a clear solution. So we dissolve 6.2 g of $Ca(NO_3)_2$ and 0.8 g of $LiNO_3$ in 200 ml distilled water under continuous stirring at room temperature during 1 h. The urea solution $CH_4N_2O$ has been added

* kadariahmed_14@yahoo.fr
* ahmed.kadari27@gmail.com
* ahmed.kadari@univ-tiaret.dz

 

drop wise to the above solution. Different quantities of manganese acetate $Mn(CH_3CO_2)_2.2H_2O$ (0.002 g, 0.016 g and 0.032 g) were added to form three doped $CaLi_2O_2$ clear transparent solutions. In order to obtain our samples in powder form, the solutions were dried at 100 °C for 72 h to evaporate the contained water and to remove organic compounds. The resulting powders were grinded with mortar-pastel and then calcined in an electrical furnace at 400 °C for 4 h. The flowchart for the preparation of pure and manganese ($Mn^{2+}$) doped calcium lithium $CaLi_2O_2$ nanoparticles is shown in Fig. 1.

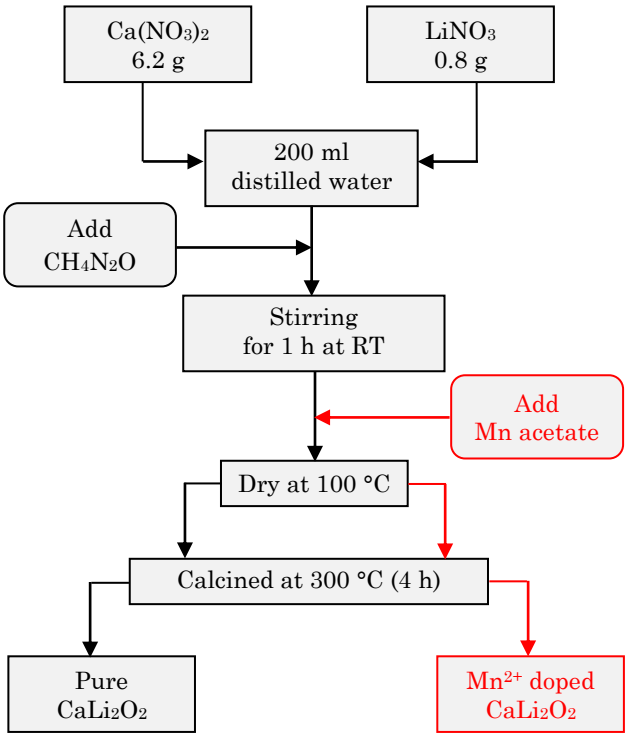


**Fig. 1** – Flowchart for the preparation of Mn doped $CaLi_2O_2$ nanoparticles

### 2.3 Powder Characterization

The phase composition of our calcium lithium oxide nanoparticles were analyzed by X-ray diffraction (XRD) (MiniFlex 600 powder diffractometer with CuK$\alpha$ radiation, $\lambda = 1.5406$ Å, in the range from 3° to 90°); optical properties were studied using SHIMADZU (UV-1650-PC) double beam spectrophotometer. FT-IR spectra were recorded by using Alpha Bruker FT-IR spectrometer.

## 3. RESULTS AND DISCUSSION

### 3.1 UV-Visible Spectroscopy

In order to study the effect of $Mn^{2+}$ doping on the optical response of $CaLi_2O_2$, UV-Visible transmittance measurements were taken in the range of 200-900 nm at room temperature. Fig. 2 shows the RT transmittance spectra of pure $CaLi_2O_2$ and $Mn^{2+}$ doped $CaLi_2O_2$ nanoparticles. All samples exhibit better transmittance (between 95 % and 98 %) in the visible region indicating good transparency of the studied samples. Among the different $Mn^{2+}$ concentrations, 0.002 g-doped sample shows a strong transmittance (95 %) in the visible region. It can be observed that the transmittance decreases with the increase in the doping concentration. The variation of absorption coefficients as a function of energy is shown in Fig. 3.

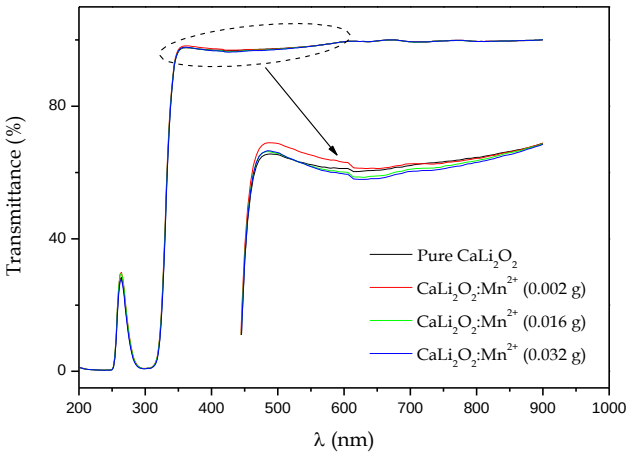


**Fig. 2** – UV-Visible transmittance spectra of pure and $Mn^{2+}$ doped $CaLi_2O_2$ nanoparticles: (black line) pure $CaLi_2O_2$; (red line) $CaLi_2O_2$:$Mn^{2+}$ (0.002 g); (green line) $CaLi_2O_2$:$Mn^{2+}$ (0.016 g) and (blue line) $CaLi_2O_2$:$Mn^{2+}$ (0.032 g)

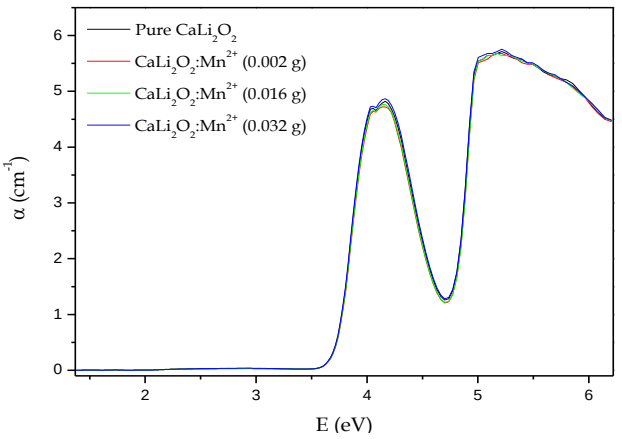


**Fig. 3** – Variation of absorption coefficient as a function of energy for pure and $Mn^{2+}$ doped $CaLi_2O_2$ nanoparticles: (black line) pure $CaLi_2O_2$; (red line) $CaLi_2O_2$:$Mn^{2+}$ (0.002 g); (green line) $CaLi_2O_2$:$Mn^{2+}$ (0.016 g) and (blue line) $CaLi_2O_2$:$Mn^{2+}$ (0.032 g)

The optical band gap values of pure $CaLi_2O_2$ and $Mn^{2+}$ doped $CaLi_2O_2$ nanoparticles have been calculated by using the Tauc's formula which explains a relationship between the absorption coefficient ($\alpha$) and incident photon energy ($h\nu$) [14]:

$$\alpha h\nu = A(h\nu - E_g)^n,$$

where $A$ is a constant and $E_g$ is the optical band gap of the sample. The coefficient $n$ is taken as ½ since these are direct allowed transitions. The band gap (can be obtained by plotting a graph $(\alpha h\nu)^2$ versus $h\nu$ and extrapolating linear portion of the absorption edge. The calculated band gap by the Tauc's plot for all samples is shown in Fig. 4.

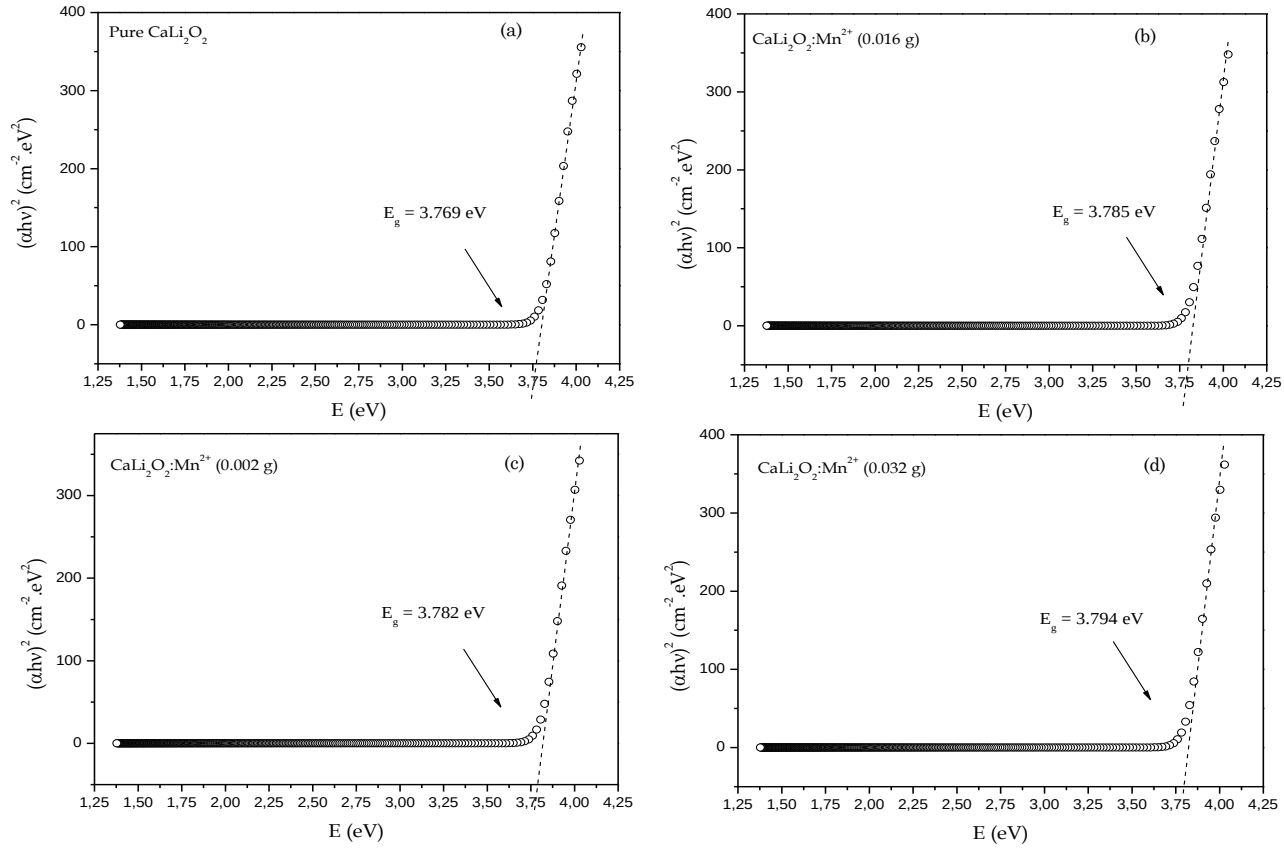


**Fig. 4** – The plot of the optical density versus energy: pure $CaLi_2O_2$ (a), $CaLi_2O_2:Mn^{2+}$ (0.002 g) (b), $CaLi_2O_2:Mn^{2+}$ (0.016 g) (c) and $CaLi_2O_2:Mn^{2+}$ (0.032 g) (d)

The variation of the band gap energies as a function of the doping $Mn^{2+}$ content is shown in Fig. 5. It can be seen from the figure that the band gap energies ($E_g$) of $CaLi_2O_2$ nanoparticles increase from 3.769 to 3.794 eV for the pure and the strongly doped samples, respectively. This variation is due to the quantum confinement effect. We add also that the increase in the $E_g$ values may be due to the decrease in crystallite sizes of synthesized nanoparticles with the increase in manganese concentration in $CaLi_2O_2$ matrix.

The continuous red shift of the band gap by Mn-doping is due to the direct energy transfer between semiconductor-excited states and the 3*d* levels of $Mn^{2+}$ ions.

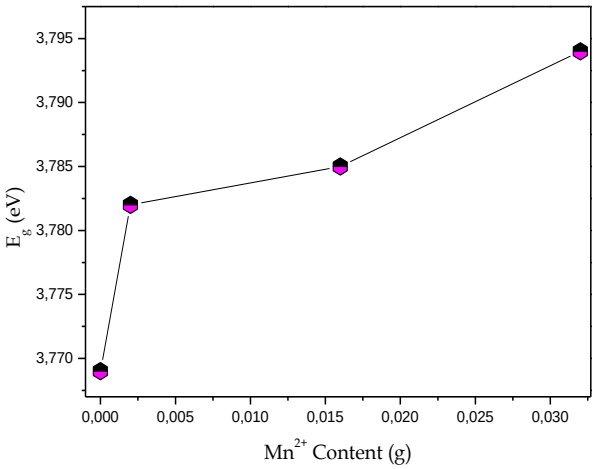


**Fig. 5** – Variation of the band gap energies as a function of the doping $Mn^{2+}$ content

We know that a band gap is an energy region with no allowed states. The density of states versus energy depends on the chemical composition of the material. If the chemical composition is changed, at least, in principle, the state density distribution should change. Doping is the action to add impurities, so, the chemical composition changes by doping. A change in the energy distribution of the allowed states cannot have a general rule, such as the band gap will increase after the introduction of impurities. Generally, these impurities are called dopants, which create allowed shallow states in the band gap. Shallow states have low ionization energies; and, when the doping density is high, the dopant states generate a band. If this band is very close to the valence or conduction band edge, the band gap will increase.

### 3.2 X-Ray Diffraction (XRD)

The crystal structure of the prepared samples was taken by using powder X-ray diffractometer. XRD patterns are used to study the structure of the crystalline material, size, phase, and interplanar distance. Fig. 6 shows the XRD patterns of $CaLi_2O_2$ nanoparticles prepared from precursor solutions using sol-gel process. The presence of diffraction peaks at $2\theta$ values approximately equal to 32.38°, 35.53°, 36.98°, 41.34°, 53.20°, 60.46° and 63.61° indexed to (100), (101), (200), (102), (220), (102) and (311) planes has been confirmed by the JCPDS Card No. 4-777.

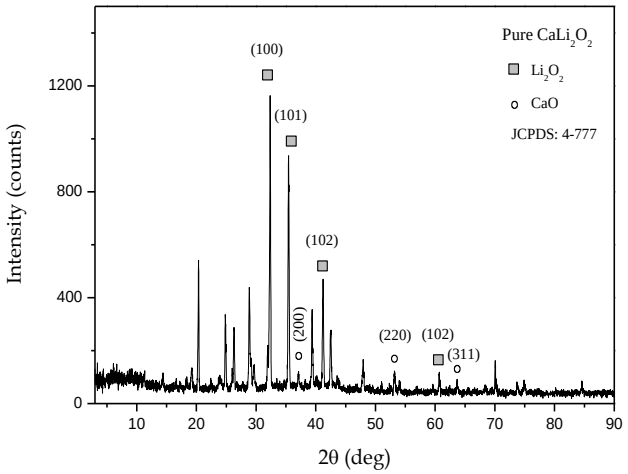


**Fig. 6** – XRD patterns of pure $CaLi_2O_2$ nanoparticles prepared by sol-gel method

The superposition of XRD patterns of pure and Mn-doped $CaLi_2O_2$ nanoparticles is shown in Fig. 7.

The only observed remark here is the extinction of the main diffraction peak (at $2\theta = 32.38°$), following the increase in the $Mn^{2+}$ content in the $CaLi_2O_2$ matrix. This may be due to the difference in atomic radius between $Ca^{2+}$ (180 pm), $Li^{2+}$ (145 pm) and $Mn^{2+}$ (140 pm) ions. We can also suggest that some manganese ($Mn^{2+}$) ions go to the interstitial sites.

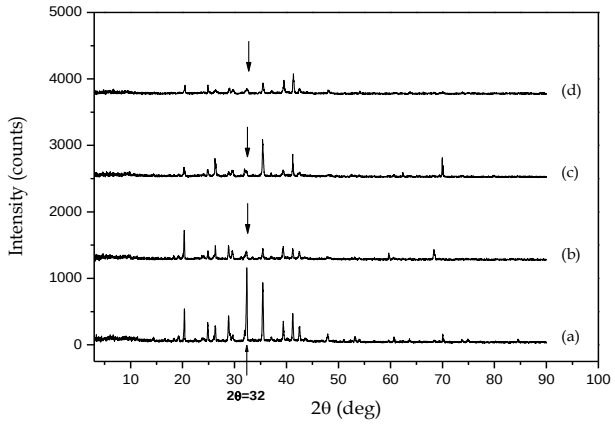


**Fig. 7** – XRD patterns of pure and $Mn^{2+}$ doped $CaLi_2O_2$ nanoparticles prepared by sol-gel process: pure $CaLi_2O_2$ (a), $CaLi_2O_2$:$Mn^{2+}$ (0.002 g) (b), $CaLi_2O_2$:$Mn^{2+}$ (0.016 g) (c) and $CaLi_2O_2$:$Mn^{2+}$ (0.032 g) (d)

The crystallite sizes ($D$) were calculated from the main diffraction peak ($2\theta = 32.38°$) using the Debye-Scherrer formula [15]:

$$D = \frac{0.9\lambda}{\beta.\cos\theta},$$

where $\lambda$ is the wavelength of the X-ray used (1.5406 Å), $\beta$ is the full width at half maximum of the main diffraction peak ($2\theta = 32.38°$).

The variation of this microstructural parameter as a function of $Mn^{2+}$ doping content is shown in Fig. 8. It is observed that the crystallite size decreases with an increase in the $Mn^{2+}$ concentration in our synthesized $CaLi_2O_2$ matrix. This remark may explain the change in the structure and extinction of the main diffraction peak shown above. The crystallite size depends directly on the crystallographic axes and $Mn^{2+}$ doping level and indirectly on the synthesis process, calcination temperature and solution concentration.

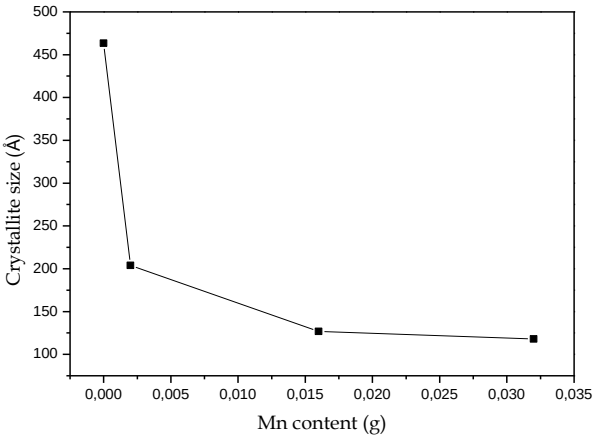


**Fig. 8** – Variation of crystallite size ($D$) as a function of $Mn^{2+}$ doping content

### 3.3 FT-IR Spectroscopy

Fourier transform infrared spectroscopy was used to determine the functional group and vibrating bonds of the sample. It is used as an additional technique to obtain information regarding chemical bonding and to evidence the presence of organic and inorganic species, such as OH groups. Fig. 9 shows the FT-IR spectra of our synthesized $CaLi_2O_2$ nanoparticles in the wavenumber range from 4000 to 400 $cm^{-1}$. Samples studied here have been thermally treated at 300 °C.

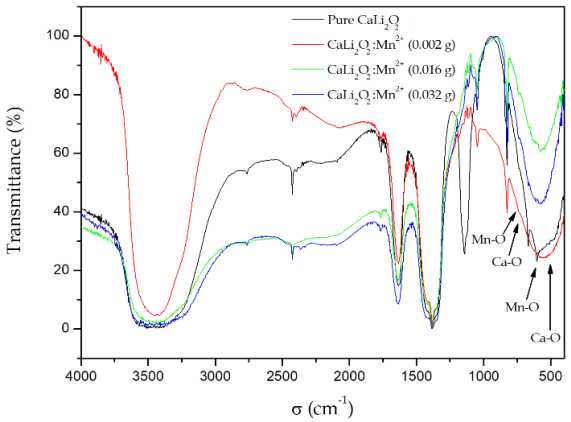


**Fig. 9** – FT-IR spectra of pure and $Mn^{2+}$ doped $CaLi_2O_2$ nanoparticles prepared by sol-gel process

The bands due to Mn–O–Mn linkages were predicted in the region 584-601 $cm^{-1}$ [16]. The band at 713 $cm^{-1}$ is related to Ca–O bonds. The wide and strong band at around 500 $cm^{-1}$ corresponds to the Ca–O bonds [17]. The weak peak at 745 $cm^{-1}$ has been attributed to the Li–O vibration [18].

## 4. CONCLUSIONS

In conclusions, pure and $Mn^{2+}$ doped $CaLi_2O_2$ nanoparticles have been synthesized by sol-gel method. The

Fourier transform infrared (FT-IR) spectroscopy, the UV-Visible (UV-Vis) spectroscopy and the X-ray diffraction (XRD) confirm that $Mn^{2+}$ ions have been successfully incorporated into the $CaLi_2O_2$ matrix. The band gap energy of nanoparticles increased from 3.769 eV to 3.794 eV with an increase in manganese concentration; this was attributed to the quantum confinement effect and to the decrease in crystallite sizes. The crystallite sizes of our synthesized nanoparticles have been decreased from 463 Å to 117 Å with the increase in $Mn^{2+}$ concentration. The only observed remark in the XRD patterns was the extinction of the main diffraction peak (at $2\theta = 32.38°$), following the increase in the $Mn^{2+}$ content in the $CaLi_2O_2$ matrix, this is caused by different atomic radius of chemical elements $Ca^{2+}$, $Li^{2+}$ and $Mn^{2+}$.

## ACKNOWLEDGEMENTS

The authors would like to acknowledge the General Direction for Scientific Research and Technological Development (DGRSDT), Algeria, for the financial support of this work.

## REFERENCES

1. R.S. Watkins, A.F. Lee, K. Wilson, *Green. Chem.* **6**, 335 (2004).
2. G. Tilekar, K. Shinde, K. Kale, R. Raskar, A. Gaikwad, *Front. Chem. Sci. Eng.* **5** No 4, 477 (2011).
3. A.M. Goncalves, R.A.B. Lima-Corrêab, J.M. Assaf, A.R.A. Nogueira, *Catal. Today.* **279**, 177 (2017).
4. M. Mohamed, S. Yusup. A.T. Quitain, T. Kida, *Environ. Sci. Pollut. Res.* **26**, 1 (2018).
5. D. Drdlik, M. Slama, H. Hadraba, K. Drdlikova, J. Cihlar, *Ceram. Int.* **44**, 2884 (2018).
6. P. Sakthivel, S. Muthukumaran, *Opt. Laser. Technol.* **103**, 109 (2018).
7. G. Ravi-Kumar, Ch. Srinivasa-Rao, M.C. Rao, *Optik.* **170**, 156 (2018).
8. M. Sayed et al., *J. Mol. Liq.* **272**, 403 (2018).
9. I. Devadoss, S. Muthukumaran, *Mat. Sci. Semicon. Proc.* **41**, 282 (2016).
10. M.L. Madugu, O. Olusola, O. Echendu, *J. Elec. Materi.* **45**, 2710 (2016).
11. M. Wan, K. He, H. Hong, Q. Wang, Q. Chen, *Physica. B.* **547**, 111 (2018).
12. J.R. Salasin, C. Rawn, *Ceramics.* **1**, 175 (2018).
13. *Nanomaterials in the Wet Processing of Textiles* (Ed. N. Vigneshwaran, V. Prasad, A. Arputharaj, A.K. Bharimalla, P.G. Patil) (Sweden: Scrivener Publishing LLC: 2018).
14. D. Fadil, R.R.F. Hossain, G.A. Saenz, A.P. Kaul, *J. Mater. Chem. C.* **5**, 5323 (2017).
15. S. Ravi Shankar, A.R. Balu, M. Anbarasi, V.S. Nagarethinam, *Optik.* **126**, 2550 (2015).
16. K. Linganna, M. Rathaiah, N. Vijaya, C. Basavapoornima, C. Jayasankar, S. Ju, W.T. Han, V. Venkatramu, *Ceram. Int.* **41**, 5715 (2015).
17. M. Galván-Ruiz, J. Hernández, L. Baños, J. Noriega-Montes, M.E. Rodríguez-García, *J. Mater. Civil. Eng.* **21** No 11, 625 (2009).
18. J. He, X. Song, W. Xu, Y. Zhou, M. Rettenmayr, *Mater. Lett.* **94**, 176 (2013).

## Вплив заміщення $Mn^{2+}$ на оптичні властивості нових наночастинок $CaLi_2O_2$, синтезованих методом золь-гелю

A. Kadari[1], A. Azaiz[2], N. Mokhtari[1], D. Horri[1]

[1] *Engineering Physics Laboratory, University of Tiaret, Algeria*
[2] *Synthesis and Catalysis Laboratory, University of Tiaret, Algeria*

Нова наночастинка на основі композитного оксиду кальцію і літію $CaLi_2O_2$ була успішно синтезована за допомогою методу золь-гелю. Метою роботи є вивчення зміни оптичних властивостей зі зміною концентрації іонів $Mn^{2+}$ у наночастинках $CaLi_2O_2$. Новизною цього дослідження є синтез наночастинок $CaLi_2O_2$, легованих Mn. Для вивчення їх фізичних властивостей отримані зразки у вигляді порошку термічно обробляли при 300 °C, а потім характеризували порошковою рентгенівською дифракцією (XRD), УФ та видимою (UV-Vis) спектроскопією та інфрачервоною спектроскопією з перетворенням Фур'є (FT-IR). Рентгенограми показують, що кристалічна структура змінювалася зі зміною концентрації іонів $Mn^{2+}$ в решітці $CaLi_2O_2$. Включення атомів марганцю в $CaLi_2O_2$ підтверджено FT-IR. Це можна пояснити появою деяких смуг поглинання в діапазоні хвильових чисел від 584 до 601 $см^{-1}$. Розмір частинок зменшується з 463 Å до 117 Å. Значення ширини забороненої зони змінювалося від 3,769 до 3,794 еВ, що було пов'язано з ефектом квантового обмеження.

**Ключові слова:** Золь-гель, $CaLi_2O_2$, Легування $Mn^{2+}$, Заборонена зона.